

# Experimental Study on Steel Structural Frame Connected by Beam-Column Joints by Nonlinear Elastic Hysteresis Hinge

**Akihiko OBATA, Tetsuya NISHIDA & Jun KOBAYASHI**

*Department of Architecture & Environment Systems, Akita Prefectural University*

**Naofumi TERAMOTO**

*Department of Civil and Environmental Engineering, Akita National College of Technology*



## SUMMARY:

The elastic-hinge joint system is considered as the structural frame with nonlinear elastic hysteresis. This joint system shows a nonlinear elastic restoring force-rotation relation and it can realize origin-oriented frames. Nonlinear elastic hysteresis ensures the elasticity of structural components such as beams and columns, even during the occurrence of a massive earthquake. Therefore, such structural components should not be expected to absorb seismic energy. The dissipation of seismic energy is efficiently controlled by utilizing some devices such as a dumper or additional components that can be replaced easily.

The objective of the present study is to investigate the effect of massive earthquakes on a steel structural frame having the proposed elastic hinge-joint system, by performing a substructure pseudo-dynamic test. The test results clarify the nonlinear elastic hysteresis characteristics of the relation between moment and rotation angle at the joint. These characteristics of the joints agree with the predicted theoretical model.

*Keywords: steel structural frames, nonlinear elastic hysteresis, substructure pseudo-dynamic test*

## 1. INTRODUCTION

The two main purposes of the nonlinear elastic hysteresis characteristic are to increase the deformation limit value, which can ensure that columns, beams, and other primary members are within their elastic range even if a major earthquake strikes, and to enlarge the deformation region so that damage to the whole structure is limited to minor damage and the structure easily recovers its pre-earthquake state. In conventional column-to-beam joints, seismic resistance of a structure is expected from the energy absorption capacity, and plastic deformation of the joints is tolerated. As a result, residual deformation occurs in the frame, and it is highly likely that reuse of the building will be problematic. However, in elastic-hinge joint systems, proactive use is made of the plasticization of replaceable members and the damping devices for energy absorption, whereas only the stiff and load-carrying elements are loaded in the columns, beams, and other primary structural members, thus preventing residual deformation due to the yield in the structural members. Because column and beam elements and joints are kept within their elastic range, it is possible to reuse the buildings after an earthquake. In these “elastic-hinge joint systems,” proposed by Yamada et al.<sup>1)-5)</sup>, the origin-oriented, nonlinear elastic hysteresis characteristic is a distinctive hysteresis characteristic.

**Figure 1** is a schematic diagram showing the application of an elastic-hinge joint system to a column-to-beam joint. This elastic-hinge joint system is also applied to the column base. In the case of **Figure 1**, the beams are pressure joined using wire rods (connection bolts), which pass through the column and possess high strength and a wide elastic range. An initial tension of approximately half of the elastic limit strength is applied to the connection bolts. In response to an earthquake of medium size or smaller, the joints act as rigid connections due to the initial tension of the connection bolts. In response to a stronger earthquake, rotation occurs due to separation between the connection surfaces of the column and the end of the beam, making use of the high elasticity of the connection bolts; however, even in this case, the yield of the members is limited to a very small range of sites that

transmit the compressive force associated with separation and that become the axes of rotation. The connection bolts always remain within their elastic range.

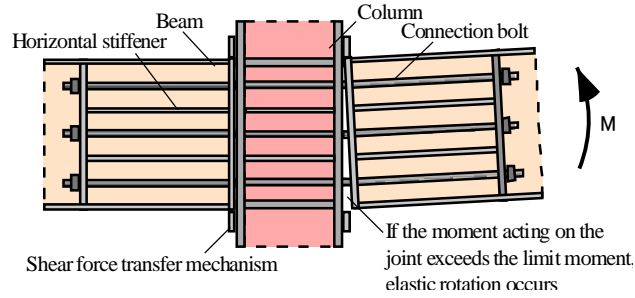


**Figure 1.** Schematic of an elastic-hinge joint system

In addition to elastic-hinge joint systems, numerous results from research addressing similar issues have already been published<sup>6),7)</sup>. One aspect that all of this research seems to have in common is the attempt to enable continued use of buildings or members by limiting the damage to places other than the primary members. However, all of the construction methods considered in the research expect energy absorption by the joint components. Therefore, as a consequence of the plasticization of joint elements in which energy absorption is expected, the residual deformation in these joints is unavoidable. This research investigates the elastic-hinge joint system, in which a nonlinear elastic hysteresis characteristic can be realized without relying on plastic deformation of the joint elements for energy absorption.

Some results providing information regarding hysteresis characteristics in joints in elastic-hinge joint systems have been produced through the research carried out so far<sup>1)-5)</sup>. However, the influence of the nonlinear elastic hysteresis characteristic on the whole frame is still not fully understood. Therefore, in this research, a substructure pseudo-dynamic test was carried out using specimens of column-to-beam joints in an elastic-hinge joint system, with the aim of ascertaining the deformation properties of a whole frame model with a nonlinear elastic hysteresis characteristic. In particular, the unresolved issue of the reducing effect of the response acceleration in the frame is studied. Also, problems concerning joint deformation properties are discussed, including in particular the problem of rotational stiffness of the joint decreasing before separation<sup>5)</sup>.

## 2. JOINT CONFIGURATION AND THE HYSTERESIS CHARACTERISTIC

**Figure 2** shows a schematic of the nonlinear elastic hysteresis characteristic aimed for in this research. The nonlinear elastic hysteresis characteristic of the joint causes deformation to occur with rotation as the surfaces of the joint connection elastically separate, leading to a change in stiffness. During an earthquake of medium intensity, the joint behaves as a rigid connection without separating. As the level of the input seismic motion increases, the joint moment increases, and the joint separates when a certain limit moment is reached. After separation, the joint moment increases with rotation of the joint, but if joint components such as the beam and the connection bolts are within the elastic range at that point, the joint will behave elastically and will return to the origin on unloading with no residual deformation, even if separation and rotation occurs.

The limit load at which separation occurs is called the separation load, and the angle of rotation caused by separation is called the separation rotation angle. **Figure 3** shows a schematic of the modeling of the joint rotational spring. The separation rotation angle of the joint,  $\theta_s$ , does not increase until just before the joint moment,  $M$ , reaches the limit at which separation occurs, but after separation, it increases in accordance with the stiffness of the connection bolt. The limit moment at which separation occurs,  $M_{sep}$ , the rotational stiffness after separation,  $k$ , and the tension in the connection bolt at tier  $i$ ,  $T_i$ , can be represented by the following equations.

$$M = n \sum T_i d_i = n \sum (T_{0i} + \Delta T_i) d_i \quad (2.1)$$

$$M_{sep} = n \sum T_{0i} d_i \quad (2.2)$$

$$k = (n A_K E_K / L_K) \sum d_i^2 \quad (2.3)$$

$$T_i = T_{0i} + \Delta T_i = T_{0i} + (A_K E_K / L_K) d_i \theta_S \quad (2.4)$$

$d_i$  : Distance  $i$  from axis of rotation to tier  $i$  connection bolt

$n$  : Number of connection bolts in each tier

$T_0$  : Initial tension applied to connection bolt       $A_K$  : Cross-sectional area of connection bolt

$E_K$  : Young's modulus of connection bolt       $L_K$  : Effective length of connection bolt

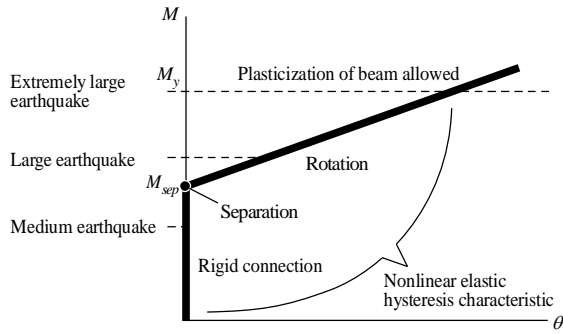


**Figure 2.** Schematic of the nonlinear elastic hysteresis characteristic of a joint

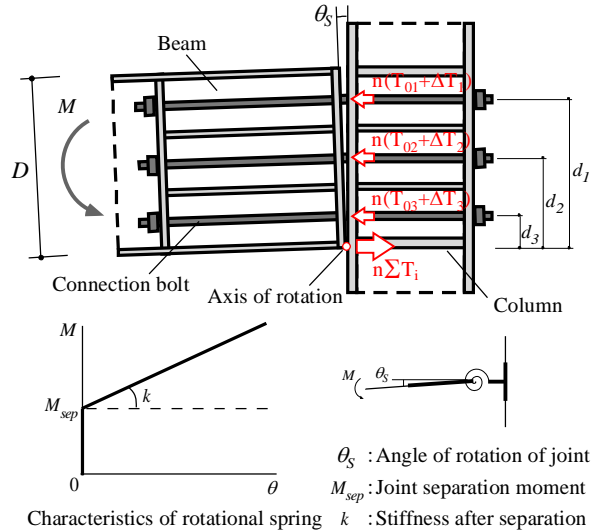


**Figure 3.** Modeling of the joint rotational spring

The nonlinear elastic hysteresis characteristic permits compressive plasticization of the beam flange during an extremely large earthquake. Even in this situation, the connection bolts behave elastically, and brittle collapse of the frame is prevented by the transfer of stress at the joining surfaces via the connection bolts.

### 3. OUTLINE OF SUBSTRUCTURE PSEUDO-DYNAMIC TEST

#### 3.1. Test frame

**Figure 4** shows the frame model and elevation schematic of the test frame. The frame is assumed to be a 2D steel structure consisting of nine stories and one span, and the frame model has a nonlinear elastic rotational spring for modeling the elastic hinges in the column-to-beam joints at each story and in the column base joints. The specimens representing the column-to-beam joints are Joint A and Joint B at both ends of the first-story beam shown in **Figure 4**. The first-story beam is composed of Joint A, Joint B, and part of the beam element between them. The vertical displacement and the angle of rotation at the intermediate node linking each element are used as the control displacements of the test specimen, and the shear force and the moment obtained from the specimen are fed back as restoring forces to end the force in the response calculation. Details are given in Section 3.3.

In designing the frame model, first, the cross sections of members such as columns and beams are set so that the required horizontal load-carrying capacity of each story is satisfied in consideration of a model in which rigid connections replace the nonlinear elastic rotational springs. Then, the separation load of each nonlinear elastic rotational spring is set with a target of approximately 60% of the yield moment at the edge of each member. Also, in this paper, the base shear coefficient at the required horizontal load-carrying capacity is taken as 0.25. The stiffness after separation is set so that the elastic separation rotation angle when the beam reaches its yield moment is approximately 1/50 and the story drift angle is approximately 1/25. The frame load is calculated with a unit floor load of 6.0 kN/m<sup>2</sup>. The

weight of each story is 430 kN and the total weight of the structure plane is 3870 kN. Damping is assumed to be  $h=0.03$ .

**Table 1** gives the levels of the input seismic motion and the behavior targets for the joint. The input seismic wave is a 10 second El-Centro NS wave at time interval 0.01 seconds. Because this test is a first attempt, examination of the characteristics of the input seismic wave and the influence on the frame will be a subject of future study. In this test, the maximum velocities of each input seismic wave are standardized as 25, 50, and 100 cm/s, and the waves are inputted consecutively into the frame model and specimens. (Hereafter, as shown in Table 1, the pseudo-dynamic test cycles with maximum input seismic wave velocities, standardized as 25, 50, and 100 cm/s, are called RUN 1, RUN 2, and RUN 3, respectively.) The behavior targets for the joint are as follows: a rigid connection with no separation occurring in RUN 1, the frame kept as a whole within its elastic range despite separation and rotation occurring in RUN 2, and the connection bolts kept within their elastic range while allowing a certain amount of plasticization of the beam ends in RUN 3.

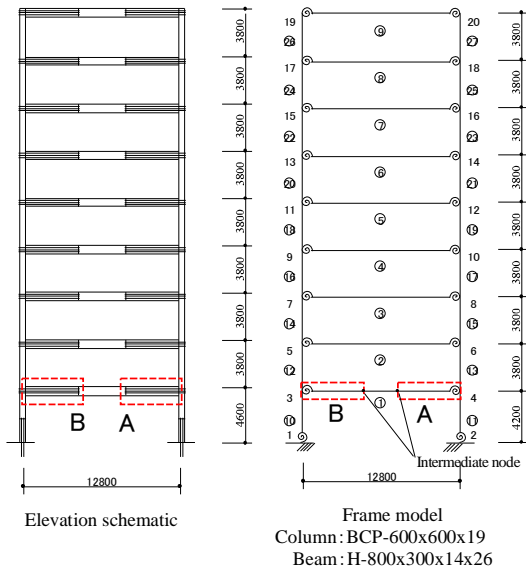


**Figure 4.** Schematic of the test frame

**Table 1.** Levels of input seismic motion

	Reference velocity	Earthquake size	Joint behavior target
RUN1	25cm/s	Level 1 Medium earthquake	Rigid connection
RUN2	50cm/s	Level 2 Large earthquake	Separation rotation permitted
RUN3	100cm/s	Level 3 Extremely large earthquake	Elastic range (beam yield permitted)

### 3.2. Specimens of tested part

**Figure 5** shows a schematic of the loading system, and **Figure 6** shows a schematic of a specimen. On the basis that the specimen is equivalent to 1/3 of the frame model, H-250x125x6x9 is used for the beam and H-300x300x10x15 for the column. As shown in **Figure 6**, the beam is installed vertically and, via an endplate (PL-268x125:  $t=19$ ) welded to the end of the beam, it is pressure joined to the horizontal column using six PC steel rods (connection bolts). After a prescribed initial tension has been introduced into the PC steel rods, the specimen is installed in the loading system. The column is secured to the test floor using a column holding jig and anchor bolts. The top end of the specimen beam is secured to the loading beam, after which the horizontal displacement and angle of rotation are applied to the top end of the beam. Using the load cell installed in each jack, the moment at the intermediate node side and the beam shear force in the specimen part of the frame model shown in **Figure 4** are measured. Tension in the PC steel rods is measured by affixing strain gauges. The top and bottom edges of the beam flanges, which form the rotation centers of the joint, require reinforcement, as compressive stress is thought to concentrate there during separation rotation. In this test, the joint rotation centers are reinforced by welding a compression pivot reinforcing plate all around the beam flange surface from the joint connection surface up to 200 mm. Beam yield is considered to occur beyond the confines of the reinforcing plate, and so a strain gauge is affixed to the beam flange at a point 250 mm from the joint connection surface. Rotation occurring as a result of separation of the joint is measured by installing two displacement gauges on the flanges near the joint, as shown in the enlargement of Area A in **Figure 6**, and dividing the difference in displacement measured by these gauges by the distance between the gauges. **Table 2** shows the material

characteristics of the specimen beam and PC steel rod bolt used in this test, and **Table 3** lists the specimens. There are four types of specimens in total, and the experimental variables are the effective length of the PC steel rods,  $L_k$ , and the presence or absence of steel strips inserted into the joint. **Figure 7** depicts the steel strip insertion. The steel strip has dimensions of 200 mm length, 6 mm thickness, and 25 mm width, and it is inserted at the locations of the compression pivots of the specimen joint, as shown in the figure. Past research<sup>4)</sup> has clearly demonstrated that inserting a steel strip at the locations of the compression pivots restricts the transfer of compressive stress during separation to a small area at the edge of the endplate, and so mitigates the loss of stiffness before separation. This test also examines the influence of this loss of stiffness before separation on the frame.

The initial tension in the specimen is introduced by extending the PC steel rods using a coupler, tensioning them using the jacks installed at the top end of the beam, and adjusting the nuts. The amount of tension introduced is read from strain gauges attached to the PC steel rods. In an elastic-hinge joint system, as a general rule, the amount of initial tension introduced into a connection bolt is set to approximately 50% of the elastic limit strength of the connection bolt; however, in this research, it is possible to introduce a slightly larger initial tension into the PC steel rods at the beam center tier than when the subject is a side column joint. Therefore, with the aim of ensuring a somewhat higher separation load for the test specimens, the targets for initial tension introduced are 70 kN (2600  $\mu\epsilon$ ) in the beam top and bottom tier PC steel rods (50% of the 0.2% offset yield strength), and 98 kN (3600  $\mu\epsilon$ ) in the beam center tier PC steel rods (70% of the 0.2% offset yield strength). The specimen separation moment,  $M_{sep}$ , calculated from the target initial tension is 63.8 kNm (1722 kNm in terms of the frame model), and this is equivalent to 57.3% of the yield moment at the edge of the specimen beam. Also, the margin of error of the target initial tension in all of the specimens is approximately  $\pm 5.0$  kN.

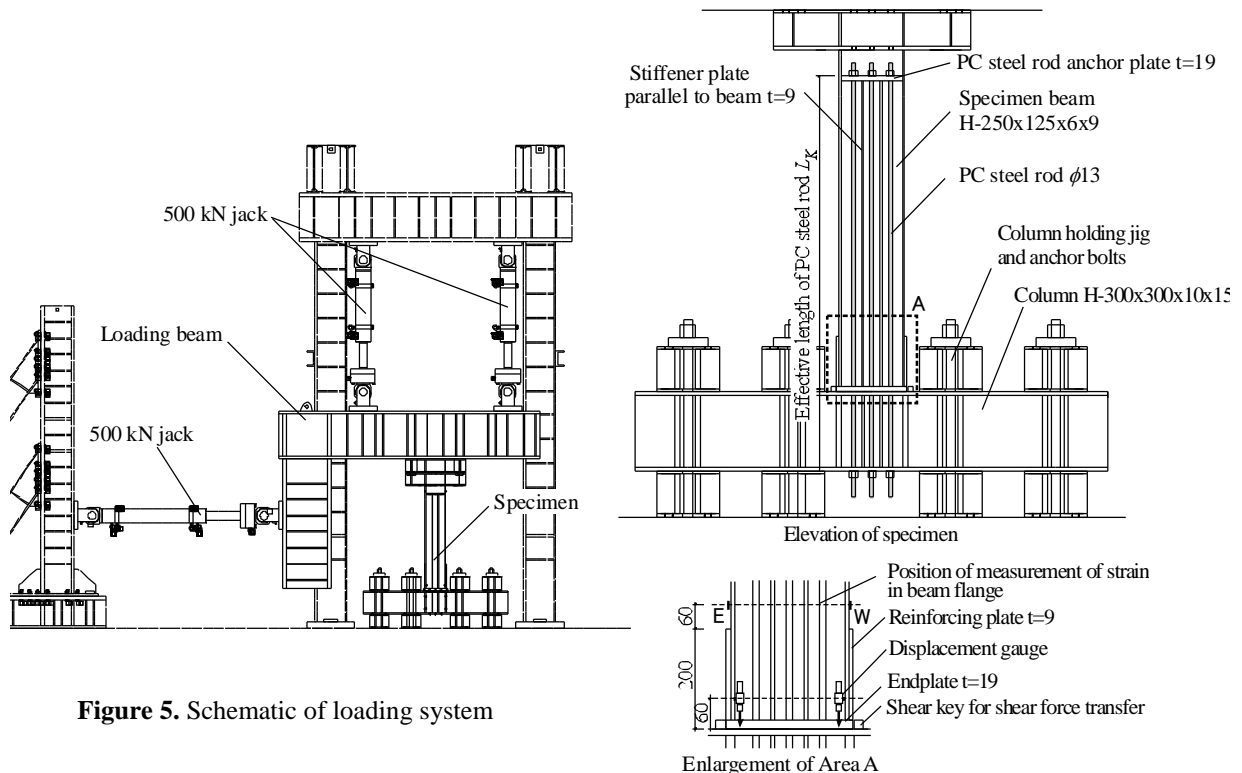


**Figure 5.** Schematic of loading system

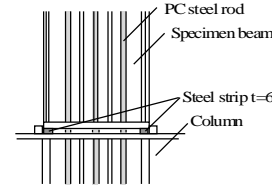
**Figure 6.** Schematic of specimen

**Table 2.** Material characteristics

	Cross-sectional area (mm <sup>2</sup> )	Moment of inertia (mm <sup>4</sup> )	Young's modulus (N/mm <sup>2</sup> )	Yield stress (N/mm <sup>2</sup> )	Yield strain ( $\mu\epsilon$ )	0.2% offset strength (kN)	Tensile strength (N/mm <sup>2</sup> )	Maximum tensile load (kN)
Specimen beam H-250x125x6x9 (SN490)	3697	3960x10 <sup>4</sup>	2.05x10 <sup>5</sup>	351	1712	141	522	151
PC steel rod $\phi$ 13 Type B, No. 1	132			1062	5180		1137	

**Table 3.** Specimen specifications

Specimen name	Effective length of PC steel rod $L_K$ (mm)	Steel strip	Stiffness after separation $k$ (kN·m)
Type-1	1500	No	$2.84 \times 10^3$
Type-1s		Yes	
Type-2	1000	No	$4.26 \times 10^3$
Type-2s		Yes	

**Figure 7.** Depiction of steel strip inserted

### 3.3. System setup of substructure pseudo-dynamic test

The test system was constructed based on the test systems used in substructure pseudo-dynamic tests carried out in past research<sup>8)</sup>. This test uses four PCs in parallel. A PC for the response calculation conducts a response analysis of the frame model and then sends the specimen target displacement at the next step, obtained from the result of the response calculation including the part subject to testing, to the PCs for the control of each specimen. Each specimen control PC, in conjunction with the force application controller and pump unit, loads the specimen up to the target displacement obtained from the response calculation. Following that, the specimen restoring forces at the target displacement are calculated by using the values from the load cells installed in each jack, and then these forces are fed back into the response calculation via the control PC. At the same time, the values from the displacement gauges and strain gauges installed on the specimen are loaded into the measurement PC. Each PC is connected by a LAN (TCP/IP), and the measurement data is stored on either the response calculation PC or the measurement PC.

The sequence of the control program in the substructure pseudo-dynamic test is shown below.

1. The target displacement (vertical displacement and angle of rotation at the intermediate node at the end of the beam) at a certain step is calculated by the response calculation PC.
2. The response calculation PC transmits the target displacement to each control PC.
3. The control PC controls the force application system (controller and pump unit), by applying force until the target displacement is reached.
4. Each load (moment and shear force at the column-to-beam joint and the intermediate node from the load on the horizontal jack and two upper vertical jacks) at the time that the target displacement is reached is fed back to the response calculation PC as a restoring force.
5. At the same time that the restoring forces are fed back to the response calculation PC, the response calculation PC sends a command to begin data measurement to the measurement PC.
6. The measurement PC acquires data from the displacement gauges and strain gauges. The response calculation PC returns to Step 1 and conducts a response calculation for the next step based on the fed-back restoring forces.

Pseudo-dynamic tests that measure restoring forces through real force application cannot accommodate convergence calculations because the restoring forces are history-dependent. However, the risk in using an explicit integration method, which obtains restoring forces without relying on convergence calculations, is that the solution will diverge unless a sufficiently small integration time is set for the natural period of the subject structure. The method of numerical integration used for this test is an operator-splitting (OS) method<sup>9)</sup>. In the OS method, history-dependent nonlinear stiffness is divided into the stiffness of the history-independent linear part and the stiffness of the history-dependent nonlinear part. By using the average acceleration method of numerical integration to integrate the linear part, and a conditionally stable predictor-corrector method on the nonlinear part, a stable solution can be obtained as long as the stiffness of the linear part is not lower than the stiffness of the nonlinear part.

In this test, the OS method is adopted due to the stability of the numerical integration but, particularly during loading steps in which the response deformation increases, the effect of the this unbalanced moment manifests substantially. This unbalanced moment effect is discussed in Section 3. Also, when the OS method is used, it is difficult to eliminate the effect of the unbalanced moment at each step, and further study into methods of reducing this effect is necessary.

## 4. RESULT

The experimental results are shown below. In this test, a particularly large difference in specimen deformation properties was not found between the specimens replacing Joint A and Joint B. In this paper, results concerning specimen deformation properties are shown for Specimen A only as the representative.

### 4.1. Examination of relationship between joint moment and separation rotation angle

**Figure 8** shows the relationship between the joint moment and the separation rotation angle for each level of input seismic motion. The thick dashed gray lines in the figure indicate the results of theoretical calculations determined using the formulae shown in Chapter 2. From the figure, it is found that generally the stiffness decreases after separation for all specimens and levels of input seismic motion, and nonlinear elastic behavior is confirmed. For all of the specimens tested, it is possible to confirm the linear behavior in RUN 1 and the increasing separation rotation in RUN 2, while for RUN 3, the joint behavior conforming to the design criteria is confirmed, since the depicted history is close to the second-order gradient of the theoretical calculation results. From the figure, at each level of input seismic motion in the Type-1 and Type-2 specimens, joint rotation occurs at stages where the joint moment is small. This phenomenon was also confirmed in prior static loading tests on elastic-hinge joint systems<sup>4)</sup>, and it is thought to be caused by generation of the separation process by out-of-plane deformation of the endplate. However, this effect is small in the Type-1s and Type-2s specimens, in which a steel strip was inserted into the joint, and compared to Type-1 and Type-2 specimens, the behavior tends to be close to the theoretical calculation results. Specifically, it is thought that steel strip insertion restricts the sites where compressive stress is transferred from the beam flange to the column and mitigates the loss in stiffness before separation.

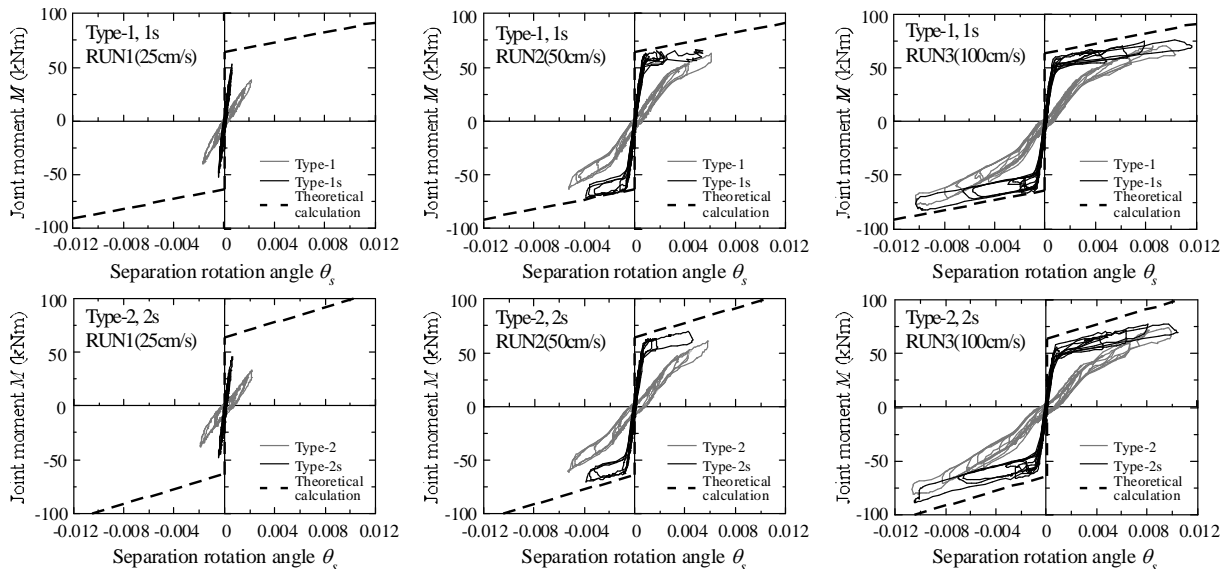


**Figure 8.** Relationship between joint moment and separation rotation angle

### 4.2. Examination of changes in the PC steel rod strain during the tests

**Figure 9** shows the relationship between joint moment and PC steel rod strain through the series of tests from RUN 1 to RUN 3. For all of the test specimens and at all levels of input seismic motion, the strain in the PC steel rods is within the elastic range and no residual strain develops. It can be confirmed that the increase in PC steel rod strain grows after the separation moment reaches approximately 63.8 kNm, and the PC steel rods stretch with separation. Even within the range where the joint moment is small (rigid connection range), the strain in the top and bottom tier PC steel rods fluctuates, and this is considered to be because the PC steel rods stretch and contract due to rotation of the beam at the PC steel rod anchor plate position. This phenomenon has little effect on the strain in

the center tier PC steel rods. For all of the specimens, it is confirmed that the strain in the PC steel rods decreases with each repetition of input from RUN 1, RUN 2, to RUN 3. When the average of the differences is taken between the start of RUN 1 and the start of RUN 3 for the strain in all of the PC steel rods in each specimen, the results are  $56 \mu\epsilon$  for Type-1,  $95 \mu\epsilon$  for Type-2,  $140 \mu\epsilon$  for Type-1s, and  $189 \mu\epsilon$  for Type-2s. This shows that the decrease in strain in the PC steel rods is particularly striking in the Type-1s and Type-2s specimens, which have a steel strip inserted into the joint, compared to the decrease in strain in the Type-1 and Type-2 specimens. On the joint connection surface in the Type-1s and Type-2s specimens, there is a slight dent from the steel strip on the endplate, and it is thought that, as a result, the initial tension is reduced.

### 4.3. Examination of plasticization of a beam member

**Figure 10** shows the relationship between the joint moment and the beam flange strain through the series of tests from RUN 1 to RUN 3. From the figure, the compressive strain increases greatly in the Type-1s, Type-2, and Type-2s specimens and leads to the beam yield. However, the beam flange strain in the Type-1 specimen remains within its elastic range and the yield is not identified. For the beam flange strain in the specimens at the start of the test, the value of the compressive strain is larger in the Type-1s and Type-2s specimens, which have the steel strip inserted, compared that of the Type-1 and Type-2 specimens, and it is evident that the compressive strain increases because the stress transfer is concentrated in the beam flange. This increase in compressive strain leads to the beam yield in the Type-1s specimen, and the loss in stiffness before separation is mitigated as a result of insertion of the steel strip; however, because the beam flange strain increases, it seems possible that plasticization of the beam flange will occur even earlier than the input level assumed during the design.

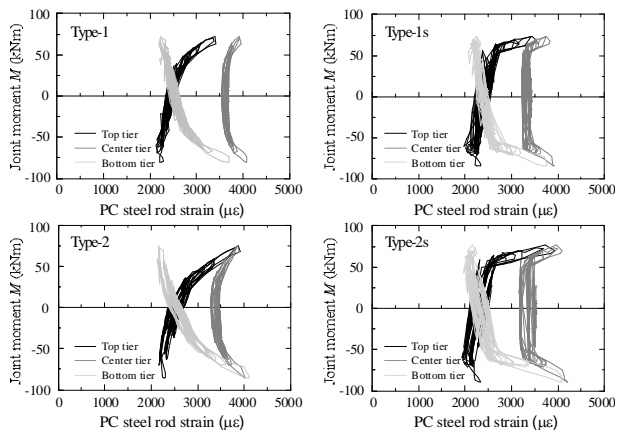


**Figure 9.** Relationship between joint moment and PC steel rod strain

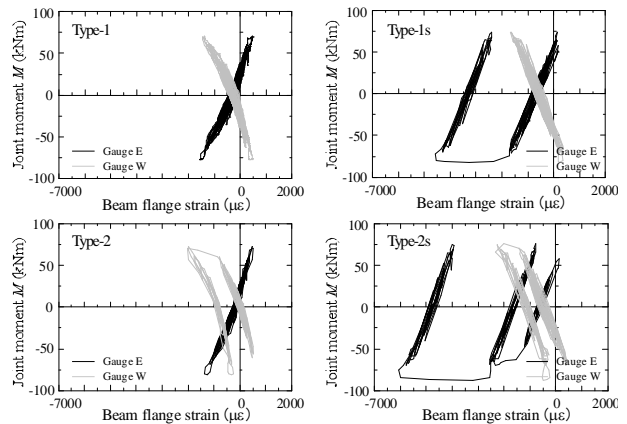


**Figure 10.** Relationship between joint moment and beam flange strain

### 4.4. Examination of relationship between story shear force and drift angle on the first story of the frame model

**Figure 11** shows the relationship between the story shear force and the drift angle on first story of the frame model. The gray dashed lines in the figure show the static incremental analysis results calculated separately for the frame model. The analysis method proposed in Reference<sup>3)</sup> was used for the static incremental analysis. The experimental results and the static incremental analysis results show a generally good correlation. At the level of the input seismic wave of RUN 2 and RUN 3, the story shear force has an erratic history. This is considered to be due to the effect of the unbalanced moment during numerical integration of the specimen part. Elimination of unbalanced moments is a subject for future study, but it is considered possible to curb the effect to a certain extent through processing, such as making the time intervals even smaller in steps where the displacement increments are large.

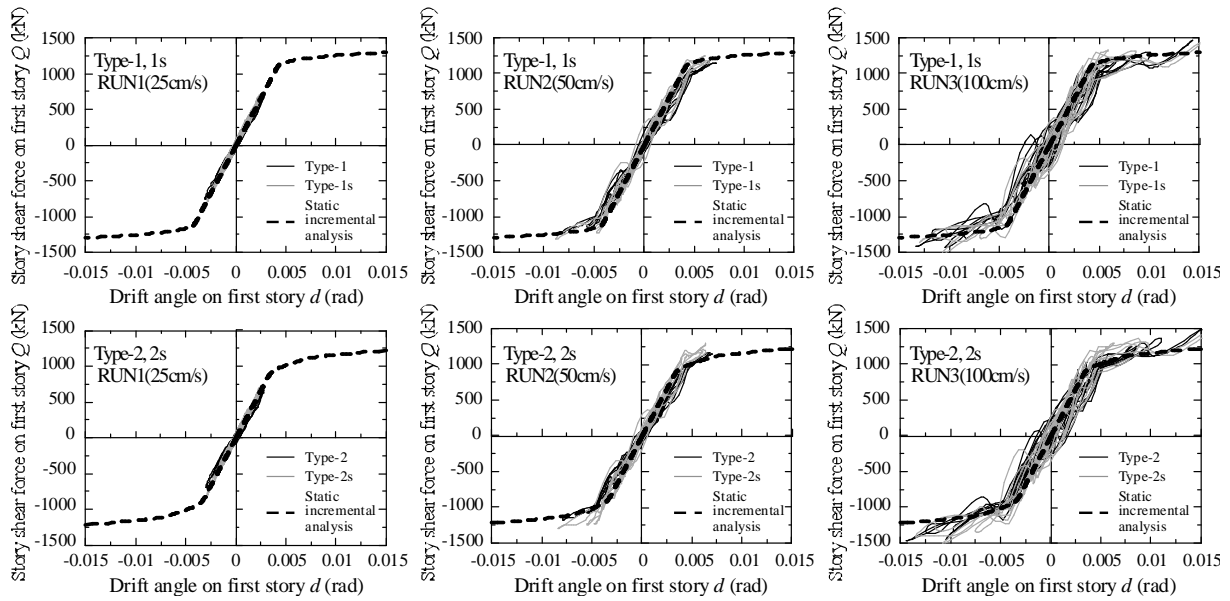


**Figure 11.** Relationship between story shear force and interstory drift angle on the first story of the frame model

#### 4.5. Examination of distribution of maximum story shear force and maximum response acceleration of frame model

**Figure 12** shows distributions of the maximum story shear force and the maximum response acceleration in the frame model subjected to testing. The white symbols are experimental results, and the black symbols are results obtained by the response analysis using a frame-only linear elastic model with the nonlinear elastic rotational spring removed from the frame model shown in **Figure 4**. It is found that, in RUN 1, in which separation of the frame model beam does not occur in any of the specimens, the frame model experimental results and the linear elastic response analysis results are in close agreement. The results for RUN 2 and RUN 3, in which separation of the joint does occur, show that the story shear force from the experimental results is lower than the linear elastic response analysis results, and the story shear force decreases as a result of the separation. With regard to the maximum response acceleration, the experimental results for RUN 3 are small at Floor 4 and above, compared to the results of the linear elastic response analysis, and the fall in the response acceleration is thought to influence the story shear force. The maximum response acceleration distributions for RUN 3 show that, in the linear elastic response analysis results, the response acceleration at Floor 2 is the lowest and, although there are some exceptions, the trend for the response acceleration is to increase with increasing floor number, whereas, in the experimental results, the trend is different, with the response acceleration large at Floor 2 and Floor R and small at the intermediate floors. This is thought to be because the frame stiffness falls due to separation rotation. The response acceleration

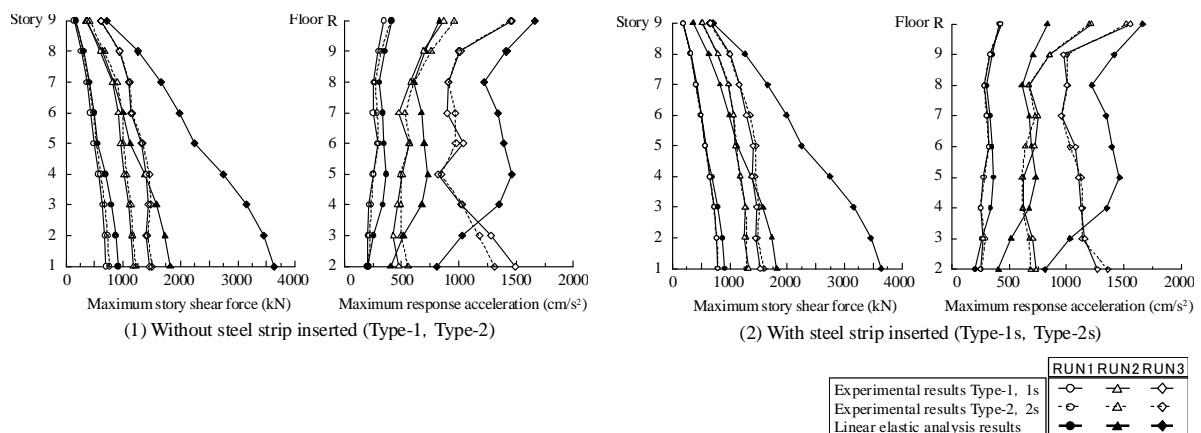


**Figure 12.** Distribution of maximum story shear force and maximum response acceleration

distributions of Type-1s and Type-2s specimens, which have the steel strips inserted, show that response acceleration increases across all floors compared to that of the Type-1 and Type-2 specimens in RUN 2. The story shear force distribution also increases in RUN 2. The values are almost the same in RUN 3, and it can be said that during an extremely large earthquake, joint rotation before separation does not greatly influence the story shear force distribution in the frame.

## 5. CONCLUSIONS

A substructure pseudo-dynamic test was conducted using column-to-beam joint specimens from an elastic-hinge joint system, with the aim of ascertaining the deformation properties of a whole frame model with a nonlinear elastic hysteresis characteristic. Shown below are the results obtained from this test.

1. The experimental results confirmed the nonlinear elastic behavior across the levels of input seismic motion (maximum reference acceleration: 100 cm/s) used in this test.
2. By comparing the experimental results and the linear elastic response analysis of the frame model, it was confirmed that the story shear force falls as a result of the reduction in response acceleration.
3. The experimental results for specimens with steel strips inserted at the location of the compression pivot of the specimen connection surface confirmed that insertion of the steel strips restricts the sites of compressive stress transfer and mitigates the loss in stiffness before separation.
4. From the experimental results for the specimens with steel strips inserted, it was found that insertion of the steel strips increases the strain in the beam flange, and it is possible that plasticization of the beam flange will occur even earlier than at the input level assumed during the design.
5. As a result of determining the story shear force distribution at each story by using the experimental results for the specimens with the inserted steel strips, it was found that, during an extremely large earthquake, joint rotation before separation does not greatly influence the story shear force distribution in the frame.

## REFERENCES

- 1) Obata, A., Teramoto, N., Nishida, T., Kobayashi, J. and Uematsu, Y. (2011). Substructure Pseudo-dynamic Test of Steel Structural Frame with a Nonlinear Elastic Hysteresis Characteristic (In Japanese). *Journal of Structural Engineering. Architectural Institute of Japan*. **Vol.57B**, 441-447.
- 2) Watanabe, T., Yamada, M., Obata, A. And Takizawa, K. (2003). Steel structure flame with elastic-hinge joint system (In Japanese). *Journal of Structural Engineering. Architectural Institute of Japan*. **Vol.49B**, 533-538.
- 3) Obata, A., Yamada, M., Watanabe, T. And Takizawa, K. (2003). Simplified Experiments on Steel Structure Flame with Elastic-Hinge Joint System (In Japanese). *Proceedings of Construction Steel. Japanese Society of Steel Construction*. **Vol.11**, 637-640.
- 4) Furukawa, S., Yamada, M., Obata, A. And Takizawa, K. (2005). Analysis of Steel Structure Flame with Elastic-hinge Joint System (In Japanese). *Journal of Structural Engineering. Architectural Institute of Japan*. **Vol.52B**, 351-357.
- 5) Miyamoto, Y., Obata, A., Uematsu, Y and Nigorikawa, T. (2009). Study on the Separation and Rotation Behavior of an Elastic-hinge Joint System (In Japanese). *Steel Construction Engineering. Japanese Society of Steel Construction*. **Vol.16 No.64**, 31-40.
- 6) M.M.Garlock, J.M.Ricles, R.Sause, C.Zhao, & L.W.Lu : Seismic behavior of post-tensioned steel frames, *Behaviour of Steel Structures in Seismic Areas*, Mazzolani & Trembary.
- 7) L.W.Lu, R.Sause, J.M.Ricles, & S.P.Pessiki : High performance, cost effective structural systems for seismic-resistant buildings, *Earthquake Engineering Frontiers in the New Millennium*.
- 8) Teramoto, N., Nishida, T. And Kobayashi, J. (2008). Structural Performance of Side Columns Subjected to Varying Axial Load. The 14<sup>th</sup> World Conference on Earthquake Engineering. Beijing, China.
- 9) Nakashima M. , Ishida M. , Ando K. (1990) ,Integration Techniques for Substructure Pseudo Dynamic Test : Pseudo dynamic test using substructuring techniques (in Japanese). *Journal of Structural and Construction Engineering*, **No.417**, 107-117.